Continent and Life Evolution

OPEN ACCESS
Article

Freeze–thaw-driven microstructural evolution and collapsibility of Xinjiang loess: implications for climate-sensitive continental near-surface materials

Kangze Yuan, Wanli Xie*, Jiahao Zhou, Xuanyu Gao, Xinyu Li and Qiqi Liu

***E-mail:** xiewanli@nwu.edu.cn

Received 30 March 2026; Revised 28 May 2026; Accepted 14 June 2026; Published 30 June 2026

https://doi.org/10.55092/cle20260006

Graphical Abstract

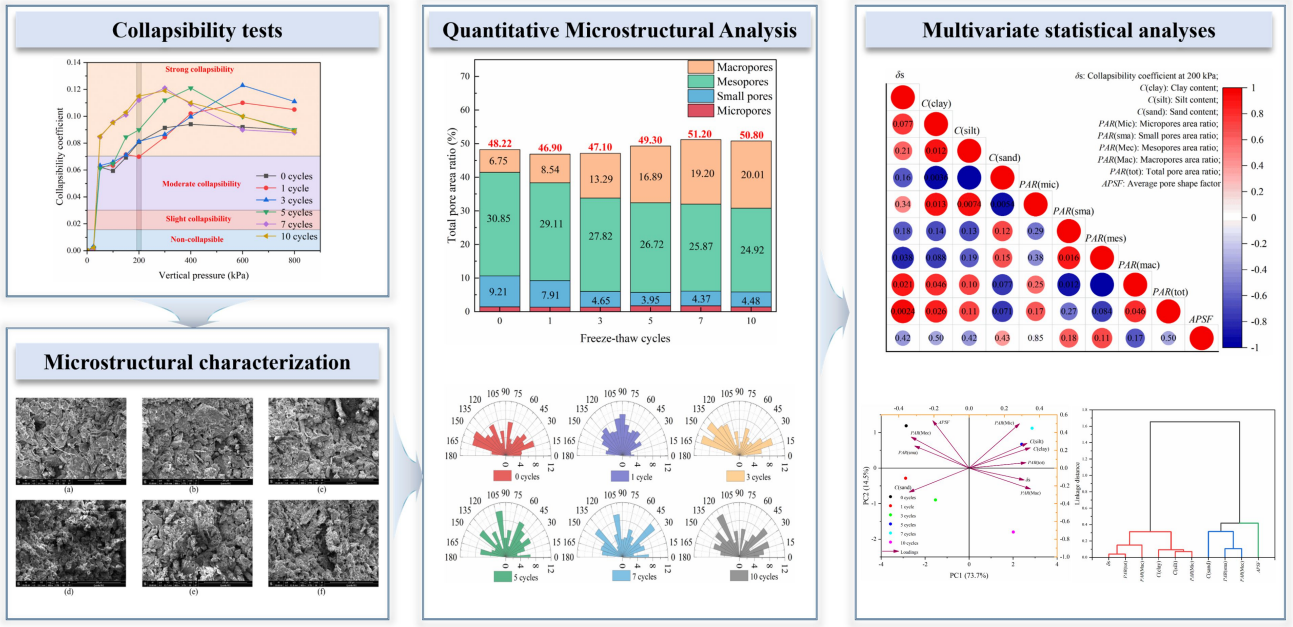

Highlights:

- Freeze–thaw cycling progressively enhanced the collapsibility of Xinjiang loess.
- A marked structural transition occurred after 5–7 freeze–thaw cycles.
- Pore-system opening and macropore growth dominated collapsibility enhancement.

Freeze–thaw-driven microstructural evolution and collapsibility of Xinjiang loess: implications for climate-sensitive continental near-surface materials

Kangze Yuan[1,2,3,4], Wanli Xie[1,2,3,4,*], Jiahao Zhou[1,2,3,4], Xuanyu Gao[1,2,3,4], Xinyu Li[1,2,3,4] and Qiqi Liu[1,2,3,4]

[1] State Key Laboratory of Continental Evolution and Early Life, Northwest University, Xi'an 710069, China

[2] Department of Geology, Northwest University, Xi'an 710069, China

[3] Xi'an Key Laboratory of Prevention of Loess Dynamic Disaster and Restoration of Environment, Northwest University, Xi'an 710069, China

[4] China-Kyrgyzstan Belt and Road Joint Laboratory on Special Geotechnical Dynamic Disaster Prevention and Control, Northwest University, Xi'an 710069, China

*E-mail: xiewanli@nwu.edu.cn.

Abstract: Loess in seasonally frozen arid regions is highly sensitive to both freeze–thaw disturbance and subsequent wetting-induced collapse, yet the microstructural pathway by which freeze–thaw cycling modifies its collapsibility remains insufficiently quantified. In this study, Xinjiang loess was subjected to 0, 1, 3, 5, 7, and 10 freeze–thaw cycles, and its collapse behavior and microstructural evolution were investigated using collapsibility tests, particle-size analysis, scanning electron microscopy (SEM), Avizo-based quantitative pore analysis, and multivariate statistical methods. The results show that freeze–thaw cycling enhanced the collapsibility of the loess, with the collapsibility coefficient at 200 kPa increasing overall from 0.0809 in the untreated state to 0.115 after 10 cycles. This response was not strictly linear: limited changes occurred after 1–3 cycles, whereas a pronounced increase in collapsibility and microstructural deterioration appeared during 5–7 cycles, indicating a transition from local freeze–thaw disturbance to more extensive structural reorganization. Repeated freeze–thaw cycling promoted aggregate disintegration and particle refinement, as reflected by increased clay and silt contents and decreased sand content. However, the enhancement of collapsibility was more closely associated with pore-system reconstruction than with particle-size redistribution alone. Quantitative pore analysis showed that the total pore area ratio increased from 48.22% to 51.20% after 7 cycles and remained high after 10 cycles, while the macropore area ratio increased markedly from 6.75% to 20.01%, accompanied by reduced mesopore content and lower pore roundness. Pearson correlation analysis, PCA, and HCA consistently indicated that total pore area ratio and macropore area ratio were the pore-related parameters most strongly associated with the collapse response, whereas particle-size redistribution and pore-shape modification played secondary roles. These findings demonstrate that freeze–thaw-enhanced collapsibility in Xinjiang loess is controlled primarily by nonlinear pore-system opening and macropore development, providing a microstructure-based explanation for the destabilization of climate-sensitive continental near-surface materials under repeated freeze–thaw forcing.

Keywords: loess; freeze–thaw cycling; collapsibility; microstructural evolution; multivariate statistical analysis

1. Introduction

Loess is one of the most widespread continental surficial deposits on Earth, covering about 10% of the global land surface and occurring extensively in semiarid to subhumid regions (Porter 2007). Owing to its high porosity, loose particle arrangement, and metastable aggregated structure, loess is highly sensitive to environmental disturbance and commonly exhibits collapse, deformation, and instability when subjected to wetting or external loading (Yang *et al.* 2022). In northwestern China, where loess is widely distributed and large-scale infrastructure increasingly extends into climatically fragile regions, such structural sensitivity has become a major geotechnical concern (Leng *et al.* 2018; Wang *et al.* 2025; Ma *et al.* 2026). In seasonally frozen loess regions, freeze–thaw cycling is an especially important environmental forcing factor. Repeated freezing and thawing can induce water migration and redistribution, weaken particle contacts, generate fissures or enlarged pores, and progressively alter the engineering behavior of loess (Zhou *et al.* 2018; Xu *et al.* 2019). Previous studies have shown that freeze–thaw cycling can significantly affect the deformation, collapsibility, void ratio, and microstructure of loess, and in some cases may trigger secondary or delayed collapse even after compaction (Li *et al.* 2018; Bai *et al.* 2024). These effects are particularly relevant in Xinjiang,

where loess deposits are exposed to strong seasonal temperature fluctuations and where shallow surficial soils frequently undergo cyclic freezing and thawing under natural conditions.

Despite this growing body of research, two important limitations remain. First, many existing studies on freeze–thaw-modified loess have focused mainly on macroscopic responses, such as strength, deformation, or bulk collapsibility, while the microstructural origin of these changes has not been fully clarified. Second, even when microstructural observations are included, the interpretation is often qualitative or based on single parameters, making it difficult to establish a systematic macro–micro linkage between structural evolution and collapse behavior. Recent work has emphasized that the alteration of loess microstructure under freeze–thaw processes is crucial for evaluating damage and instability in seasonally frozen regions (Wang *et al.* 2016; Zhao *et al.* 2023; Gao *et al.* 2025a), and that quantitative image analysis can provide more reliable structural descriptors than visual scanning electron microscopy (SEM) interpretation alone (Yuan *et al.* 2025a). From the viewpoint of loess collapsibility, this issue is particularly important. Collapsibility is fundamentally a structure-controlled behavior, and its evolution under freeze–thaw cycling cannot be adequately explained without identifying how particle composition, aggregate integrity, pore-size distribution, and pore geometry are modified during repeated environmental disturbance. SEM provides a direct way to observe the loess fabric, while image-based tools such as Avizo make it possible to extract quantitative descriptors of pore development and structural openness (Yuan and Fan 2022). Moreover, multivariate statistical approaches, including Pearson correlation analysis, principal component analysis (PCA), and hierarchical cluster analysis (HCA), offer an effective means of distinguishing the dominant structural parameters most closely associated with the collapse response (Yuan *et al.* 2025b).

Against this background, the present study investigates the effect of freeze–thaw cycling on the collapsibility of Xinjiang loess from both macroscopic and microstructural perspectives. A series of collapsibility tests were conducted on loess specimens subjected to different freeze–thaw cycles, and the associated microstructural evolution was characterized through particle-size analysis, SEM observation, and Avizo-based quantitative pore analysis. Pearson correlation analysis, PCA, and HCA were further employed to evaluate the relationships between the collapsibility coefficient at 200 kPa and selected microstructural parameters. The novelty of this study lies in explicitly identifying the nonlinear microstructural pathway through which freeze–thaw cycling enhances loess collapsibility, with particular emphasis on distinguishing the dominant role of pore-system opening and macropore development from the secondary contribution of particle-size redistribution. Unlike previous studies that mainly focused on macroscopic freeze–thaw responses or qualitative microstructural observations, this work integrates collapse testing, quantitative image analysis, and multivariate statistical interpretation to clarify the key structural controls on freeze–thaw-modified collapsibility in Xinjiang loess. Therefore, this study not only advances the understanding of loess behavior in seasonally frozen arid regions, but also provides a microstructure-based perspective for evaluating the destabilization of climate-sensitive continental near-surface materials under repeated environmental forcing.

2. Material and methodology

2.1. The study location

The loess investigated in this study was collected from Yecheng County, Kashgar Prefecture, Xinjiang, China, located at the northern piedmont of the Karakoram Mountains and near the southern margin of the Taklimakan Desert (Tian *et al.* 2026). The sampling site was selected from a representative loess slope exposure to reflect the typical near-surface loess conditions in this region. Yecheng is characterized by a warm-temperate continental arid climate with pronounced seasonal temperature fluctuations and extremely limited precipitation (Zheng *et al.* 2002). According to long-term local meteorological records, the mean annual air temperature is approximately 11.4 °C, while the mean annual precipitation is only 53.2 mm. The annual evaporation reaches approximately 2480 mm, indicating a strongly water-deficient environment. The recorded extreme air temperatures range from 39.5 °C in summer to −22.7 °C in winter. Under such climatic conditions, shallow loess deposits are frequently exposed to recurrent freezing and thawing during the cold season, making freeze–thaw action an important environmental factor governing their structural stability and hydro-mechanical behavior.

2.2. Original loess material

The tested soil corresponds to Late Pleistocene (Q_3) loess, commonly referred to as Malan loess in China (Yuan *et al.* 2024), and was sampled at depths of 1.0–1.5 m below the ground surface. Undisturbed material was trimmed and prepared into cylindrical specimens (approximately 0.10 m in diameter and 0.20 m in height) (Figure 1a). To minimize disturbance and moisture loss during transport, the specimens were sealed in paraffin-coated containers and shipped in straw-cushioned wooden crates, following established procedures (Shao *et al.* 2018). After delivery to the laboratory, the fundamental physical properties of the loess were determined in accordance with relevant ASTM test methods (ASTM 2006a), and the key parameters are summarized in Table 1.

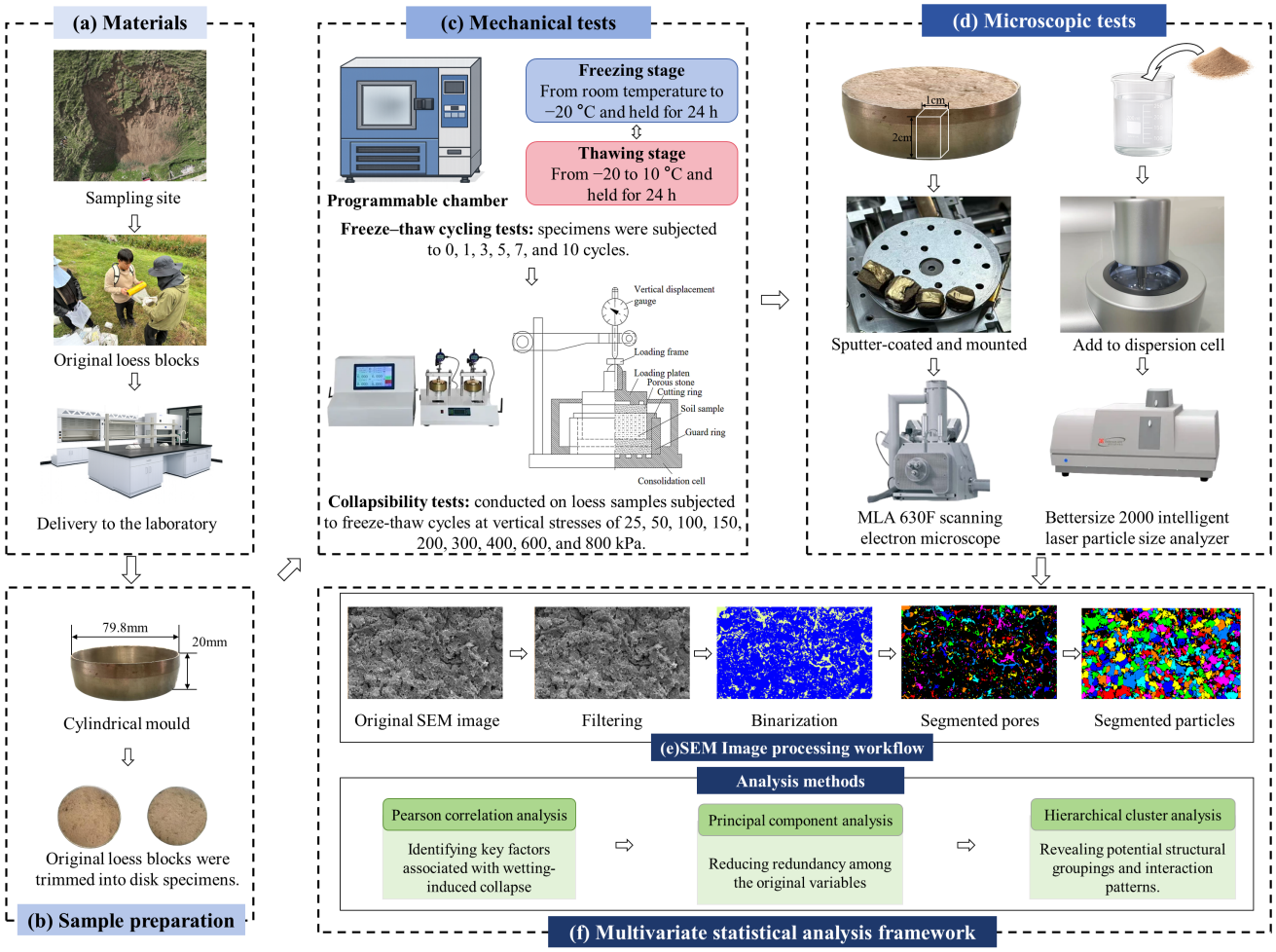

Figure 1. Flowchart of the experimental process of the study.

Table 1. Physical properties of loess.

Sample measurements	*In situ* dry density (Mg/m³)	Natural water content (%)	Specific gravity	Plastic limit (w_P/%)	Liquid limit (w_L/%)
Loess	1.16	13.7	2.71	17.7	29.1

2.3. Freeze–thaw cycling protocol

Original loess blocks were trimmed with a cutting knife to preserve the *in-situ* fabric as much as possible and then carefully shaped into disk specimens using a rigid mold (diameter 79.8 mm, height 20 mm) (Figure 1b). Immediately after trimming, each specimen was weighed, and the mass scatter was restricted to within ± 2 g across specimens (ASTM 2006b). This tight control was adopted to reduce inter-sample variability in bulk density and, consequently, to ensure that changes observed after freeze–thaw conditioning primarily reflect freeze–thaw–induced microstructural evolution rather than differences in initial specimen state. Prior to thermal conditioning, specimens were wrapped with polyethylene cling film to limit moisture exchange with the chamber atmosphere.

To capture progressive freeze–thaw damage accumulation, specimens were subjected to 0, 1, 3, 5, 7, and 10 cycles, where 0 cycles served as the untreated reference. The selected cycle numbers were designed to represent different stages of cumulative freeze–thaw disturbance rather than to reproduce a single fixed annual frequency. Specifically, 0 cycles represented the undisturbed reference condition, 1–3 cycles represented the early stage of repeated seasonal freezing and thawing, 5–7 cycles represented an intermediate stage in which cumulative structural damage may become more evident, and 10 cycles represented a more advanced disturbance condition. This design is environmentally relevant to the Yecheng area, where shallow loess deposits are exposed to pronounced seasonal temperature fluctuations and may experience repeated freezing and thawing during cold-season temperature oscillations and early-season thawing. Therefore, the selected cycle sequence provides a staged experimental framework for evaluating how progressive freeze–thaw forcing modifies the collapsibility and microstructure of near-surface Xinjiang loess. Upon completion of the prescribed cycles, specimens were removed from the chamber and immediately

transferred to subsequent laboratory testing to minimize post-conditioning moisture redistribution. Freeze–thaw conditioning was conducted in a programmable environmental chamber (temperature range approximately −30 °C to +20°C, control accuracy ±0.5 °C). The thermal boundary conditions were designed to approximate the seasonal freezing and thawing context of Yecheng, where winter air temperatures can approach −20 °C and ground temperatures during the thawing season typically recover to around 0–10 °C (Figure 1c).

One freeze–thaw cycle consisted of two sequential stages:

(i) Freezing stage: specimens were cooled from room temperature to −20 °C and held at −20 °C for 24 h, allowing the internal temperature to equilibrate and pore water to freeze sufficiently;

(ii) Thawing stage: specimens were subsequently warmed to +10 °C and held at +10 °C for 24 h to simulate thawing under early-season warming conditions.

2.4. Collapsibility tests

Collapsibility (wetting-induced collapse) tests were performed to quantify how freeze–thaw cycling modifies the collapse potential of loess (Gao *et al.* 2025b). Specimens subjected to 0, 1, 3, 5, 7, and 10 freeze–thaw cycles were tested using an Automatic Pneumatic Consolidation Instrument. For each freeze–thaw level, one double-oedometer test set was used, consisting of two companion specimens prepared from the same conditioning group: one specimen was used to determine the natural compression response, and the other was used to determine the wetting-induced collapse response under the same stress path. Therefore, the collapsibility coefficients were calculated from the paired double-oedometer measurements at each freeze–thaw level, rather than from averaged values of independent replicate test sets. To reduce the influence of initial-state variability, all specimens were trimmed from intact loess blocks, prepared with the same dimensions, and controlled within a narrow mass range before freeze–thaw conditioning. The test results were used to evaluate the systematic evolution trend of collapsibility with freeze–thaw cycling and were interpreted together with the microstructural observations and quantitative pore-structure parameters. For the reference specimen, vertical stress was applied stepwise at 25, 50, 100, 150, 200, 300, 400, 600 and 800 kPa, while vertical deformation was continuously recorded. For the wetting specimen, the sample was first loaded to a prescribed inundation stress level; subsequently, water was introduced from the specimen top to initiate wetting. The wetting-induced deformation was monitored until stabilization, defined as a deformation rate of < 0.01 mm/h. After reaching stability, the specimen was further loaded following the same incremental stress sequence as the reference specimen.

The collapse coefficient, δ_s, was calculated as:

$$\delta_s = \frac{h_0 - h_p'}{h_0} \quad (1)$$

where h_0 denotes the initial specimen height and h_p' represents the specimen height of the inundated sample at a given vertical stress level. For interpretation of the test results, the collapsibility coefficient was classified into four levels: non-collapsible ($\delta_s < 0.015$), slight collapsibility ($0.015 \leq \delta_s < 0.03$), moderate collapsibility ($0.03 \leq \delta_s < 0.07$), and strong collapsibility ($\delta_s \geq 0.07$). The collapsibility coefficient at 200 kPa was taken as the representative index for collapsibility evaluation.

2.5. Microstructural characterization

To characterize freeze–thaw–induced microstructural changes, small prismatic subsamples were extracted from the interior (central zone) of each loess specimen to minimize boundary effects (approximately 1 cm × 1 cm × 2 cm) (Figure 1d). The subsamples were fractured at mid-height to expose a fresh surface that better preserves the natural fabric and particle contacts, and the newly generated fracture surface was selected for SEM observation. The fractured pieces were mounted on SEM stubs using conductive tape and sputter-coated with a thin platinum (Pt) layer prior to imaging. SEM micrographs were acquired using an MLA 630F scanning electron microscope under consistent imaging settings across all groups. Quantitative microstructural descriptors were obtained by processing SEM images in Avizo, including image pre-processing, segmentation, and metric extraction. To ensure comparability among different freeze–thaw groups, the SEM images used for quantitative analysis were obtained from the central fractured zone of each specimen under consistent imaging conditions and at the same observation scale. Representative SEM fields were selected for each freeze–thaw level, and the same image-processing workflow was applied in Avizo for all groups. The workflow included grayscale conversion, image enhancement, noise reduction, pore–solid segmentation, and extraction of pore-structure descriptors. The preprocessing procedure, segmentation criteria, and pore-size classification thresholds were kept consistent for the untreated and freeze–thaw-conditioned specimens. This procedure was adopted to minimize operator-induced bias and to ensure that the extracted pore parameters reflected freeze–thaw-induced structural differences rather than differences caused by image processing. The detailed image-processing workflow and parameter settings follow established procedures and are provided in Yuan and Fan (Yuan and Fan 2022) (Figure 1e). The particle-size distribution (PSD) of the loess was measured by laser diffraction using a Bettersize 2000 intelligent laser particle size analyzer, covering a measurement interval from

0.02 µm to 2000 µm. PSD results were used to support interpretation of microstructural evolution and to provide baseline granulometric characteristics for all tested materials.

2.6. Multivariate statistical analyses

To quantitatively relate the wetting-induced collapse behavior of loess to its freeze–thaw-induced microstructural evolution, a multivariate statistical framework was established based on the collapsibility coefficient at 200 kPa and a set of representative microstructural parameters. The collapsibility coefficient at 200 kPa was selected as the macroscopic response index, whereas the explanatory variables included particle-size characteristics and pore-structure descriptors obtained from SEM image analysis and Avizo-based quantification. Pearson correlation analysis, PCA, and HCA were jointly employed to identify the dominant microstructural controls on collapsibility (Besson *et al.* 2020; Radelyuk *et al.* 2021). Pearson correlation analysis was first used to evaluate the linear associations between the response variable and the individual structural parameters, allowing the key factors most closely related to wetting-induced collapse to be identified (Hou *et al.* 2021). PCA was then performed to condense the high-dimensional structural dataset into a smaller number of orthogonal components, thereby extracting the principal patterns of variation and reducing redundancy among the original variables (Kim *et al.* 2013). Finally, HCA was applied to classify the variables according to their similarity in response, with the aim of revealing potential structural groupings and interaction patterns among the microstructural indicators (Tiwari *et al.* 2021). The combination of these methods enabled the macro–micro relationship governing freeze–thaw-modified loess collapsibility to be interpreted in a more systematic and quantitative manner (Figure 1f). Because the statistical dataset was established from six freeze–thaw levels, the Pearson correlation, PCA, and HCA results were used as complementary exploratory tools to identify consistent variation patterns among the selected parameters, rather than as standalone evidence for strict causal relationships. Therefore, the statistical results were interpreted together with the collapsibility tests, SEM observations, and Avizo-based pore quantification to support the proposed macro–micro mechanism.

3. Results and discussion

3.1. Effect of freeze–thaw cycles on the collapse behavior of loess

Figure 2 shows the collapsibility coefficient of Xinjiang loess under different vertical pressures after freeze–thaw cycling. Overall, freeze–thaw cycles increased the wetting-induced collapse response of the loess, although the effect varied with vertical pressure. At 25 kPa, all specimens remained non-collapsible, with collapsibility coefficients below 0.015. As the pressure increased, the wetting-induced collapse became more pronounced. Within 150–400 kPa, most specimens exhibited strong collapsibility, and the effect of freeze–thaw cycling was particularly evident. In contrast, the collapsibility coefficient at 600–800 kPa tended to stabilize or decrease slightly, indicating that the collapse response did not increase monotonically with pressure. At 200 kPa, which is commonly taken as the reference pressure for collapsibility evaluation, the collapsibility coefficient increased from 0.0809 in the untreated state to 0.115 after 10 freeze–thaw cycles, corresponding to an increase of 42.2%. Although slight fluctuations were observed at 1–3 cycles, the overall trend indicates that repeated freeze–thaw action significantly enhanced the wetting-induced collapse potential of the loess. The change in collapsibility also indicates an apparent stage-dependent response to freeze–thaw cycling. During the first 1–3 cycles, the collapsibility coefficient changed only slightly, suggesting that early freeze–thaw disturbance mainly caused local adjustment of the original loess fabric without producing a substantial increase in collapse potential. In contrast, the 5–7 cycles interval corresponded to a marked increase in the collapsibility coefficient, indicating that cumulative freeze–thaw damage had reached a stage at which local fabric disturbance was transformed into more extensive structural weakening. After 10 cycles, the collapsibility coefficient remained at a high level, but the increase became less abrupt, implying that the pore system had already undergone substantial reorganization during the intermediate freeze–thaw stage. Therefore, the 5–7 cycles interval can be regarded as a transition stage in the development of freeze–thaw-enhanced collapsibility. Repeated freezing and thawing likely weakened interparticle bonding and destabilized the original pore structure, thereby making the loess more prone to collapse upon wetting under load.

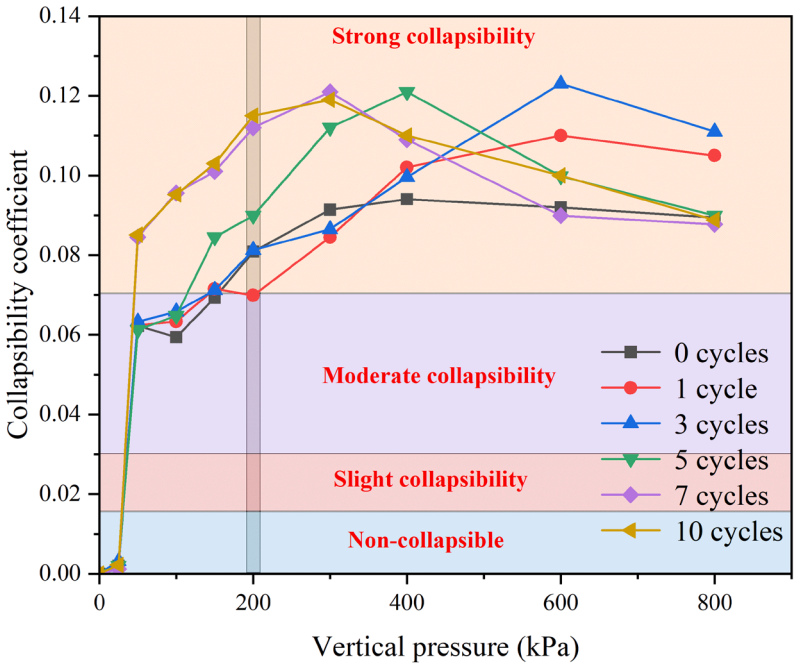

Figure 2. Collapsibility coefficient–pressure curves of loess.

3.2. Effect of freeze–thaw cycles on particle size distribution

Figure 3 presents the particle size distribution of Xinjiang loess after different freeze–thaw cycles. Under all conditions, the tested loess was dominated by silt-sized particles, indicating a typical silty loess composition. Compared with the untreated specimen, the 5- and 7-cycle groups showed an increase in clay and silt fractions and a marked decrease in sand content. The clay content increased from 5.28% to 6.49%–6.85%, whereas the sand content decreased from 14.17% to 8.99%–9.83%. This indicates that freeze–thaw cycling caused an overall refinement of the particle system, with the most pronounced effect occurring after 5–7 cycles. The distribution curves also show that the main peak shifted toward a smaller particle size after repeated freeze–thaw action, suggesting the breakdown of coarse particles or aggregates into finer particles. After 10 cycles, a slight reverse shift was observed, but the overall particle system remained finer than that of the untreated loess. This suggests that freeze–thaw-induced particle refinement was cumulative but not strictly linear. Together with the collapsibility results, these findings indicate that freeze–thaw cycling weakened the original particle framework and promoted the formation of a more unstable structure, thereby increasing the susceptibility of the loess to wetting-induced collapse.

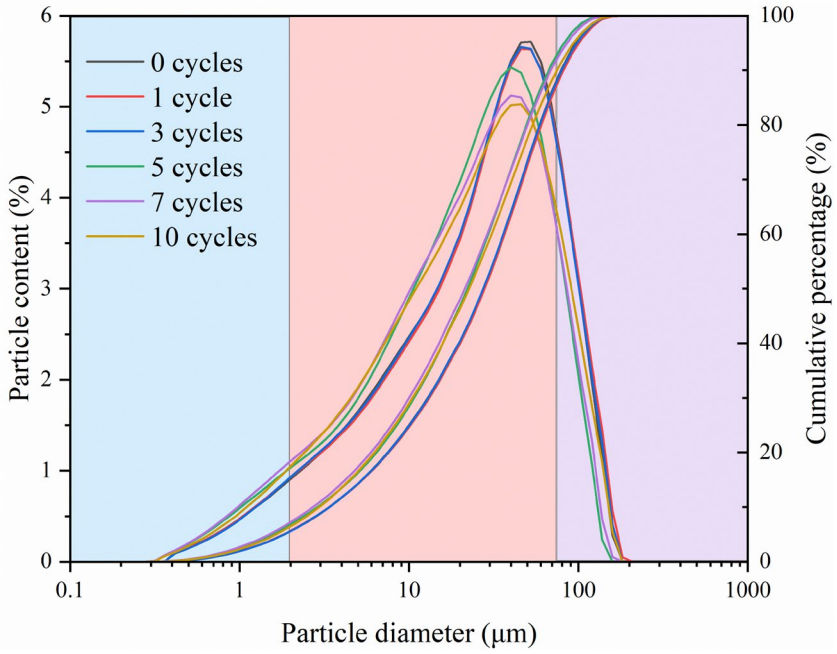

Figure 3. Particle size distribution curves of loess after different freeze–thaw cycles.

3.3. Microstructural evolution of loess under freeze–thaw cycles

Before discussing the microstructural evolution induced by freeze–thaw cycling, the basic fabric of the untreated loess should first be clarified. SEM observations indicate that the Xinjiang loess is mainly composed of silt-sized particles associated with fine clay particles, which commonly occur in the form of aggregates rather than as completely discrete grains (Figure 4). In this aggregated system, fine particles are distributed on the surfaces of larger grains or act as local bonding bridges between neighboring particles, forming a metastable soil skeleton sustained by aggregate contacts and weak cementation (Musso *et al.* 2020). Two main pore domains can be identified in this fabric, namely intra-aggregate pores and inter-aggregate pores (Vecchia and Romero 2013). The former are mainly developed within aggregates and are generally small, whereas the latter are distributed between aggregates and constitute the major part of the larger pore network (Xu *et al.* 2021). Such a microstructure, characterized by aggregated particles, abundant inter-aggregate pores, and relatively weak point or edge contacts, is typical of loess and fundamentally responsible for its high structural sensitivity. Once the original skeleton is disturbed, the unstable framework can readily undergo particle rearrangement, pore collapse, and structural compression, thereby producing significant deformation under adverse environmental conditions (Della Vecchia *et al.* 2015). Figure 4 shows the SEM images of loess after different freeze–thaw cycles. In general, freeze–thaw cycling progressively altered the original loess fabric, as reflected by aggregate breakdown, weakening of interparticle contacts, and increased structural heterogeneity. The untreated specimen showed a relatively intact aggregated structure with close particle contacts and irregular inter-aggregate pores, which is characteristic of metastable loess. After 1–3 freeze–thaw cycles, local fragmentation appeared, but the overall structure remained largely preserved. In contrast, the specimens subjected to 5–7 cycles exhibited much more evident aggregate disintegration, disordered particle arrangement, and looser contact relationships. The 7-cycle specimen showed the most pronounced structural disturbance, with fragmented aggregates and a more open pore system, indicating substantial weakening of the original soil skeleton. After 10 cycles, the structure remained highly disturbed, although local fine-particle filling and reaccumulation could be observed. This suggests that freeze–thaw-induced damage was cumulative but not strictly linear. Overall, the SEM observations indicate that repeated freeze–thaw action transformed the loess from a relatively intact metastable fabric into a looser and more unstable structure, which helps explain the increase in wetting-induced collapse after multiple cycles.

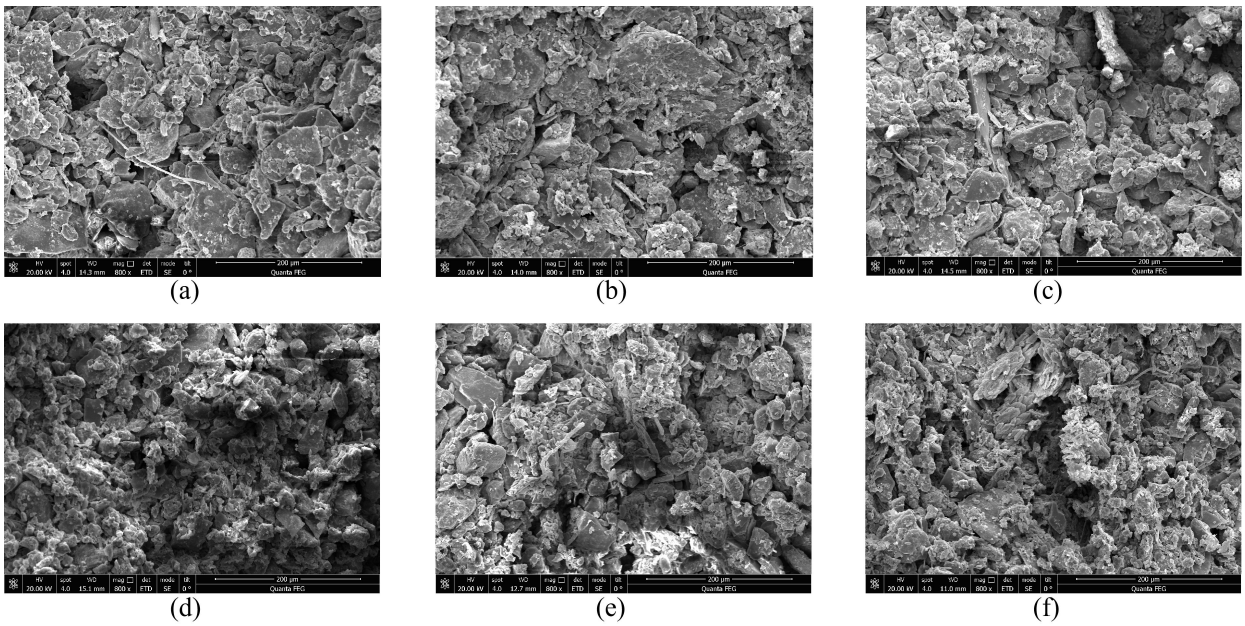

Figure 4. SEM images of Xinjiang loess after different freeze–thaw cycles. (a: 0 cycles; b: 1 cycle; c: 3 cycles; d: 5 cycles; e: 7 cycles; f: 10 cycles).

3.4. Quantitative pore-structure evolution revealed by Avizo analysis

3.4.1. Pore area ratio

To further quantify the pore-structure evolution observed in the SEM images, Avizo software was employed to extract pore characteristics from the processed micrographs. In this study, the pore area ratio (PAR) was used to characterize the proportion of pores visible within the SEM field and was calculated as

$$PAR = \frac{A_{total\ pore}}{A_{total}} \times 100\% \quad (2)$$

where $A_{total\ pore}$ is the total pore area and A_{total} is the area of the SEM image.

According to the classical pore-size classification for loess, pores were divided into four categories: micropores (0–2 μm), small pores (2–8 μm), mesopores (8–32 μm), and macropores (> 32 μm) (Lei 1987). Among them, micropores mainly occur within aggregates, whereas small pores, mesopores, and macropores are predominantly associated with inter-aggregate pores (Li *et al.* 2023). The Avizo results show that freeze–thaw cycling significantly altered the pore structure of Xinjiang loess (Figure 5). The total pore area ratio increased from 48.22% in the untreated specimen to 51.20% after 7 cycles and remained high at 50.80% after 10 cycles, indicating an overall opening of the pore system after repeated freeze–thaw disturbance. More importantly, the pore-size distribution changed markedly. Small pores and mesopores gradually decreased, whereas macropores increased sharply from 6.75% to 20.01%. This indicates that freeze–thaw cycling promoted the transformation of the original pore system toward a more open and macropore-dominated structure. The most distinct change occurred after 5–7 cycles, which is consistent with the SEM observations, the particle refinement results, and the marked increase in wetting-induced collapse during the same stage. These results suggest that repeated freeze–thaw action weakened the original aggregate framework and promoted pore enlargement, merging, and reconnection. The resulting looser and more heterogeneous pore system made the loess more susceptible to structural collapse upon wetting under load. The pore-structure results provide a microstructural explanation for the apparent transition observed in the collapsibility response during 5–7 freeze–thaw cycles. At the early stage, freeze–thaw cycling mainly caused limited pore adjustment and local aggregate disturbance, whereas the intermediate stage was characterized by a sharp increase in macropore area ratio and a simultaneous reduction in mesopore content. This indicates that the pore system did not evolve through simple uniform expansion, but through the enlargement, merging, and reconnection of existing inter-aggregate pores. Once these local changes accumulated to a sufficient degree, the original mesopore-dominated fabric was transformed into a more open and macropore-rich structure. This transition substantially weakened the ability of the loess skeleton to resist wetting-induced rearrangement under vertical loading, thereby explaining the pronounced increase in collapsibility during the 5–7 cycle interval.

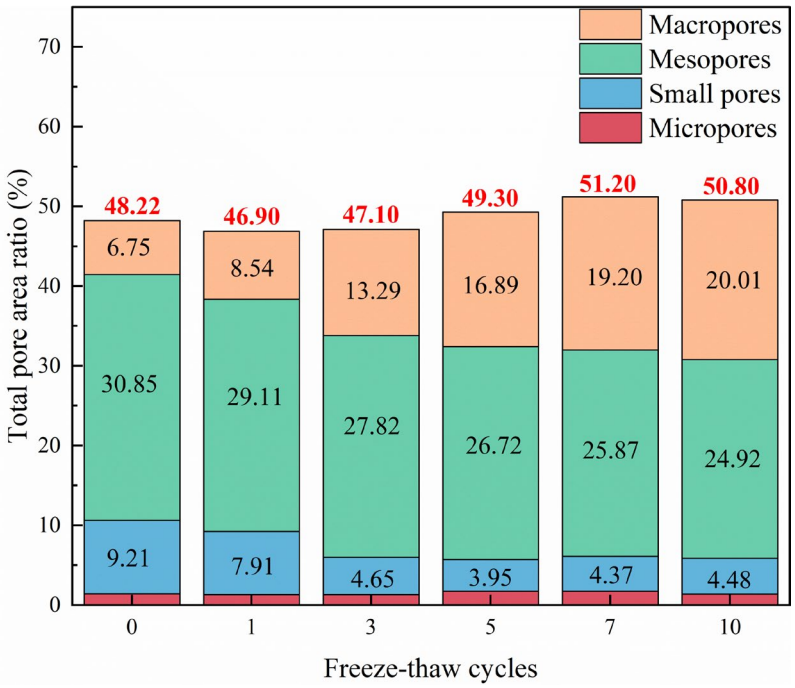

Figure 5. Histogram of the distribution of different pore categories as a percentage of the total pore area.

3.4.2. Evolution of pore roundness under freeze–thaw cycles

To further characterize the morphological evolution of pores under freeze–thaw cycling, the roundness distribution of pores extracted from the SEM images was analyzed. Pore roundness ranges from 0 to 1, with a higher value indicating a more circular pore shape and a lower value representing a more irregular pore geometry. As shown in Figure 6, pores with low roundness were dominant under all freeze–thaw conditions, and most pores were concentrated within the roundness interval of 0.15–0.35. This indicates that the pore system of the tested loess was mainly composed of irregular rather than circular pores, which is consistent with the inherently heterogeneous pore morphology of aggregated loess. With increasing freeze–thaw cycles, the proportion of low-roundness pores generally increased. In particular, the cumulative proportion of pores with roundness ≤ 0.35 increased from 67.01% in the untreated specimen to 84.38% after 5 cycles and remained high at

83.05% after 10 cycles. In contrast, the proportion of relatively high-roundness pores decreased correspondingly. This result suggests that repeated freeze–thaw action progressively transformed the pore system toward a more irregular geometry. This trend is further supported by the weighted average roundness, which showed an overall decrease from 0.341 in the untreated specimen to 0.281 after 5 cycles and 0.268 after 10 cycles, although a slight rebound was observed at 7 cycles. The overall downward trend confirms that freeze–thaw cycling progressively increased the irregularity and complexity of pore boundaries.

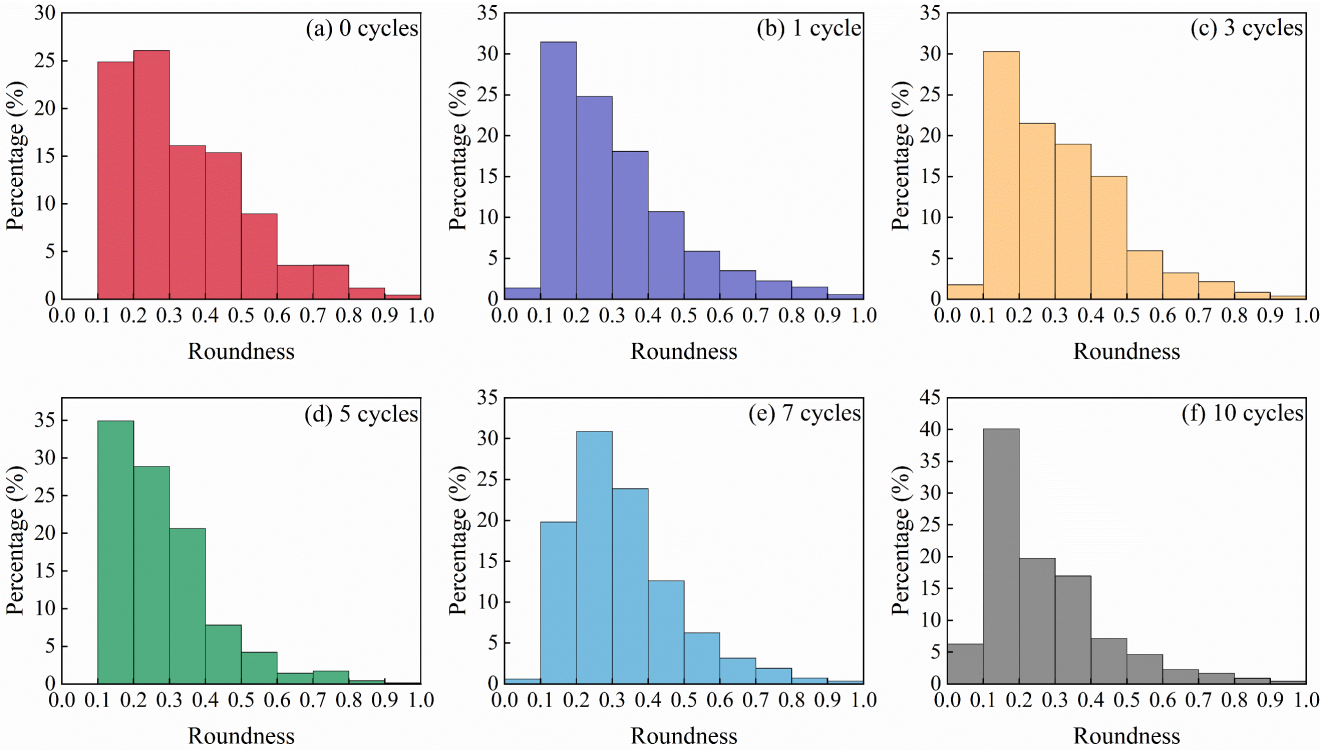

Figure 6. Distribution of pore roundness in loess under different freeze–thaw cycles.

3.4.3. Evolution of pore orientation under freeze–thaw cycles

To examine the geometric reorganization of the pore system, the orientation distribution of pores extracted from the SEM images was analyzed. The pore angle reflects the preferential direction of pore development in the two-dimensional SEM field and can therefore be used to evaluate the degree of directional arrangement and structural anisotropy of the pore network. As shown in Figure 7, the pore orientation of the untreated loess was broadly distributed over the full angular range, without a single sharply dominant direction. This indicates that the initial pore system was characterized mainly by a dispersed and heterogeneous arrangement rather than by strong directional alignment. Such a feature is consistent with the aggregated and metastable fabric of loess, in which inter-aggregate pores are irregularly distributed among structural units. After freeze–thaw cycling, the pore orientation distribution remained generally dispersed, but the fluctuation among different angle intervals became more pronounced. In several freeze–thaw groups, certain angular ranges exhibited noticeably elevated proportions, indicating the emergence of local preferential orientations. This suggests that repeated freeze–thaw action did not simply randomize the pore system, but instead promoted directional reorganization of pores during aggregate breakdown, pore enlargement, and particle rearrangement. Compared with the untreated specimen, the specimens subjected to 5–10 freeze–thaw cycles showed more evident redistribution of pore orientation, as reflected by the stronger variation in proportion across different angle classes. This indicates that the pore network became increasingly heterogeneous and structurally anisotropic after repeated freeze–thaw disturbance. Such behavior is likely associated with the preferential propagation and merging of pores along weak contact zones and unstable structural interfaces during cyclic freezing and thawing.

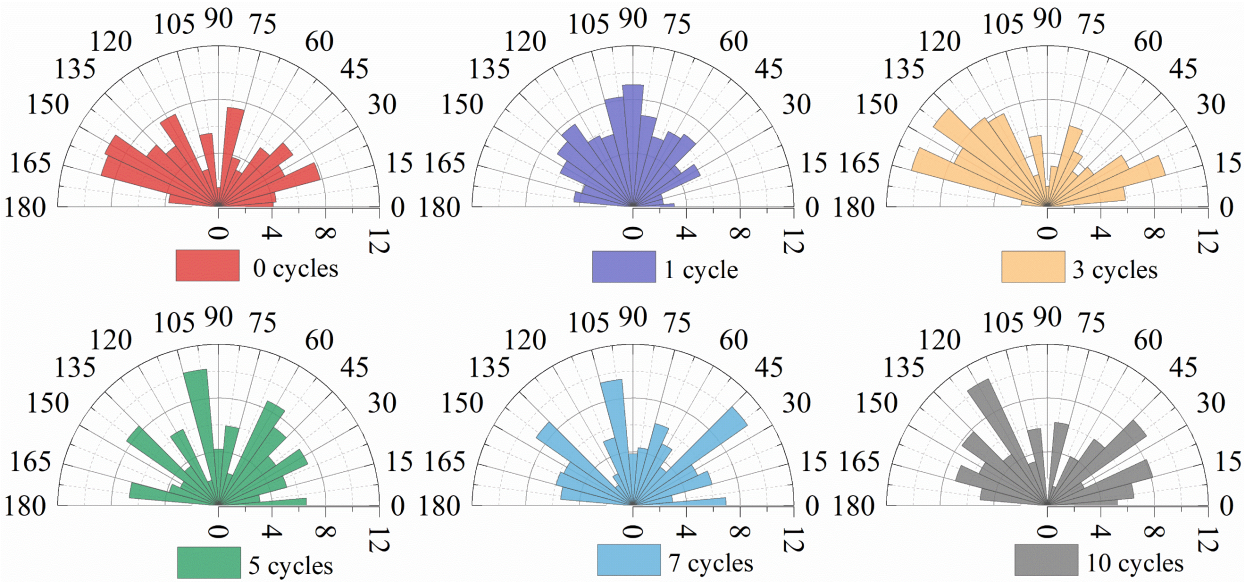

Figure 7. Rose diagrams of pore orientation in loess under different freeze–thaw cycles.

3.5. Multivariate statistical analysis

The multivariate statistical analyses were performed to explore the associations between the collapsibility coefficient and the selected microstructural parameters. It should be noted that the dataset covered six freeze–thaw levels; therefore, the statistical results are interpreted as trend-identification evidence rather than as definitive causal proof. The Pearson correlation, PCA, and HCA results were mainly used to examine whether the observed macro-scale collapse response was consistently associated with specific microstructural changes identified from SEM and Avizo analyses.

3.5.1. Pearson correlation analysis

Pearson correlation analysis was conducted to evaluate the relationships between the collapsibility coefficient at 200 kPa (δ_s) and the selected microstructural parameters (Figure 8). The results reveal that the wetting-induced collapse response was much more strongly associated with pore-structure descriptors than with the other structural variables. The total pore area ratio showed the strongest positive correlation with δ_s, followed by the macropore area ratio. In contrast, the mesopore area ratio was strongly negatively correlated with δ_s. These results indicate that the increase in collapsibility was primarily governed by the progressive opening and coarsening of the pore system, rather than by a uniform increase in all pore classes. In other words, the freeze–thaw-induced conversion of mesopores into larger and more open pore spaces played a key role in amplifying the collapse response.

Among the particle-size parameters, clay content showed a relatively strong positive correlation with δ_s, whereas sand content showed a negative correlation. This trend suggests that particle refinement, aggregate breakdown, and the weakening of the original coarse-particle framework also contributed to the increase in collapsibility. However, compared with pore-related variables, the particle-size fractions played a secondary role. In addition, the average pore shape factor was only moderately negatively correlated with δ_s, indicating that pore-shape irregularity was relevant but less decisive than pore-size redistribution and total pore development.

Overall, the Pearson correlation results support the interpretation that freeze–thaw-enhanced collapsibility was more closely associated with pore-system reconstruction, especially the increase in total pore area and macropore proportion, while particle refinement and pore-shape modification represented additional but secondary structural changes.

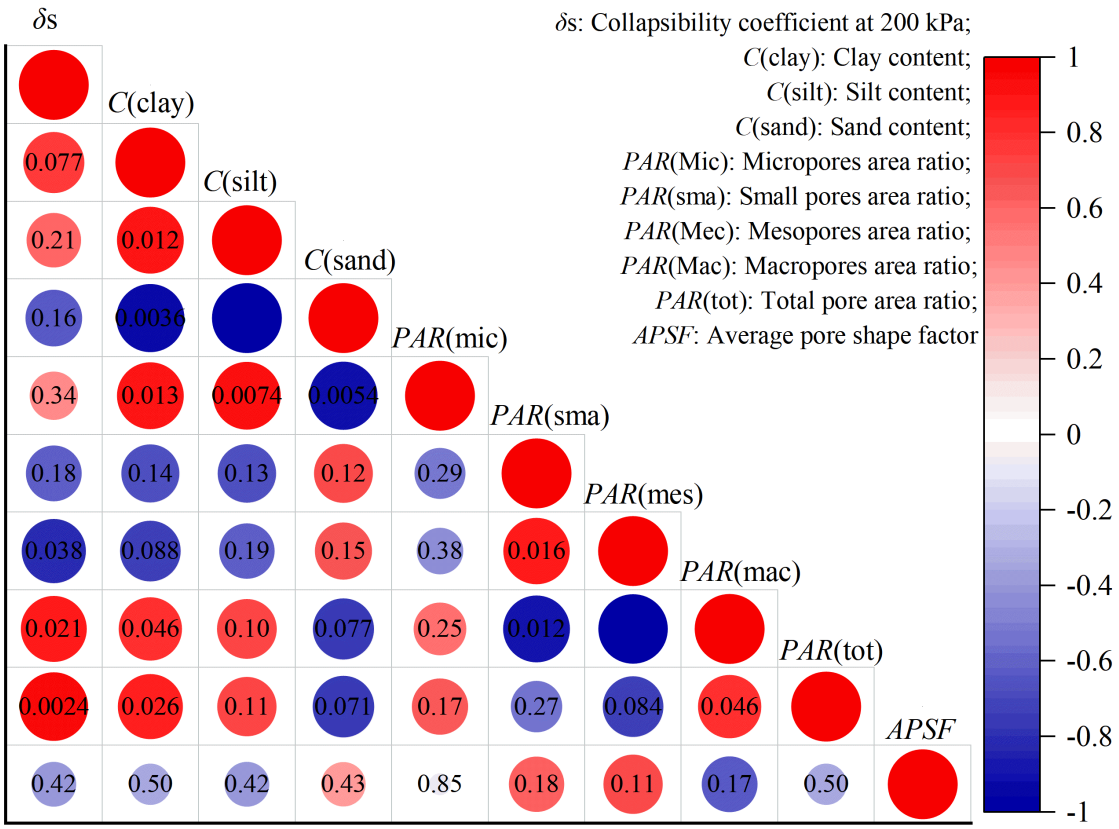

Figure 8. Pearson's correlation analysis among indicators.

3.5.2. Principal component analysis

Principal component analysis was performed to further identify the dominant structural modes governing the evolution of freeze–thaw-modified loess (Figure 9). The results show that the first two principal components explained 73.7% and 14.5% of the total variance, respectively, with a cumulative contribution of 88.2%. This indicates that the major information contained in the original microstructural dataset can be effectively represented in a two-dimensional principal component space. The loading characteristics reveal that PC1 was strongly positively associated with clay content, silt content, micropore area ratio, macropore area ratio, and total pore area ratio, while it was negatively associated with sand content, small-pore area ratio, mesopore area ratio, and average pore shape factor. Therefore, PC1 can be interpreted as a structural mode dominated by particle refinement, pore-system opening, macropore development, and increasing pore irregularity. In essence, this component reflects the progressive transition of loess from a relatively compact and mesopore-dominated structure to a more open and structurally unstable pore system under repeated freeze–thaw cycling. Compared with PC1, PC2 explained a much smaller proportion of the variance and was mainly influenced by the average pore shape factor, micropore area ratio, and mesopore area ratio. This suggests that PC2 primarily represents a secondary structural adjustment mode related to local pore-shape modification and pore-system rearrangement, rather than the dominant structural deterioration process. The score distribution of the specimens in the PC1–PC2 space shows a clear separation between the low-cycle and high-cycle freeze–thaw groups. The untreated and early-cycle specimens (0–3 cycles) are located on the negative side of PC1, whereas the specimens subjected to 5–10 cycles shift distinctly to the positive side of PC1. This result indicates that a marked structural transition occurred between 3 and 5 freeze–thaw cycles. Such a transition agrees well with the previously observed increase in macropore content, total pore area ratio, and collapsibility coefficient, as well as the SEM evidence of aggregate breakdown and pore opening at the same stage. Combined with the Pearson correlation results, the PCA results further confirm that the increase in the collapsibility coefficient at 200 kPa was governed mainly by the structural mode represented by PC1, namely pore-system opening and structural coarsening. This suggests that the enhancement of wetting-induced collapse under freeze–thaw cycling was controlled primarily by pore-network reconstruction, while particle-size redistribution and pore-shape adjustment played secondary but still relevant roles.

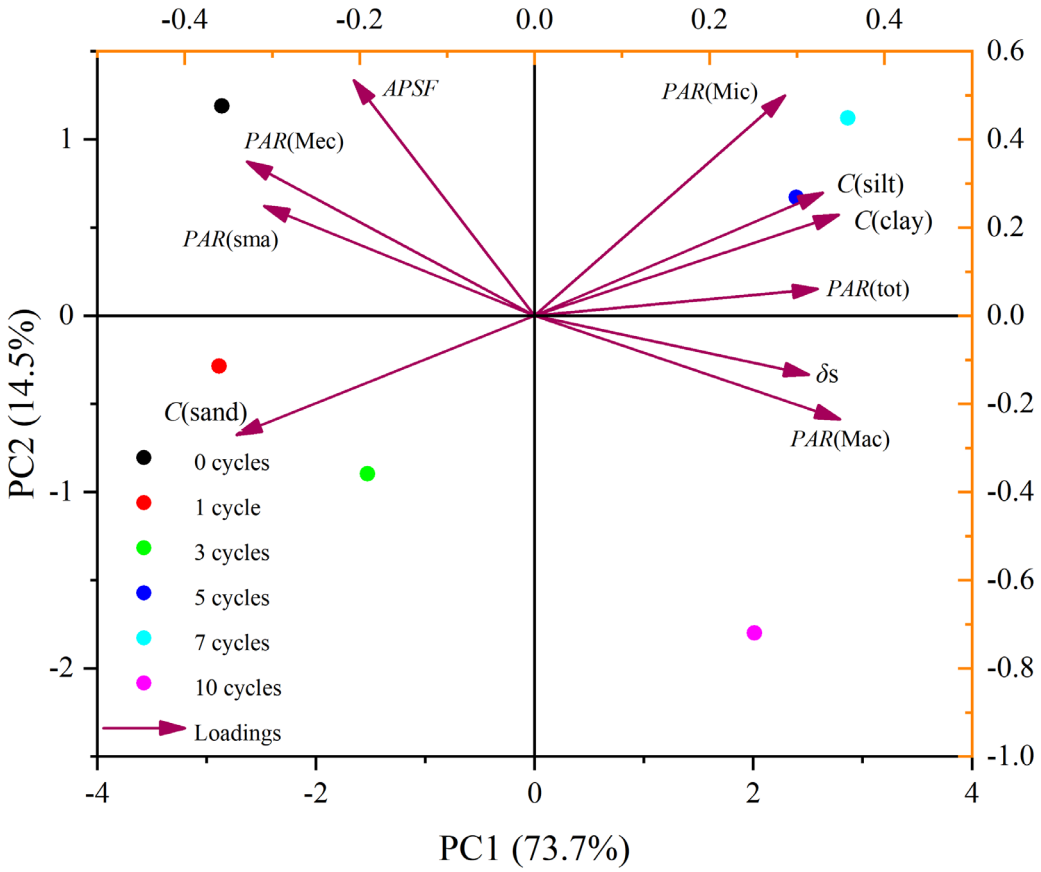

Figure 9. Biplot of PCA.

3.5.3. Hierarchical cluster analysis

HCA was conducted to further evaluate the similarity among the collapsibility coefficient at 200 kPa and the selected microstructural parameters (Figure 10). Based on the standardized dataset, the variables were grouped according to Euclidean distance using Ward's linkage method. As shown in the dendrogram, the clustering results provide an additional statistical perspective for interpreting the macro–micro relationship governing the wetting-induced collapse behavior of freeze–thaw-modified loess. At the broad clustering level, the variables were separated into two main groups. One group included sand content, small-pore area ratio, mesopore area ratio, and average pore shape factor, whereas the other group contained the collapsibility coefficient, clay content, silt content, micropore area ratio, macropore area ratio, and total pore area ratio. This division indicates that the variation pattern of collapsibility was generally closer to that of pore-opening- and fine-particle-related parameters than to that of the variables representing relatively compact structural features. A more informative interpretation was obtained when the variables were further divided into three clusters. In this case, the collapsibility coefficient was grouped directly with the macropore area ratio and the total pore area ratio, indicating that these two variables exhibited the highest similarity in variation trend with the macroscopic collapse response. Clay content, silt content, and micropore area ratio formed a second cluster, suggesting that particle refinement and local fine-scale structural adjustment constituted a secondary response group. In contrast, sand content, small-pore area ratio, mesopore area ratio, and average pore shape factor were classified into a separate cluster, reflecting a set of parameters that evolved in an opposite or weaker manner relative to the increase in collapsibility. The HCA results are highly consistent with the Pearson and PCA results. In particular, the direct clustering of the collapsibility coefficient with the macropore area ratio and the total pore area ratio further confirms that the enhancement of wetting-induced collapse under freeze–thaw cycling was governed primarily by pore-system opening and macropore development. By comparison, particle-size redistribution and pore-shape modification played secondary but still non-negligible roles. Therefore, the HCA results provide additional support for the conclusion that freeze–thaw-induced pore-network reconstruction was the dominant microstructural mechanism controlling the increase in collapsibility.

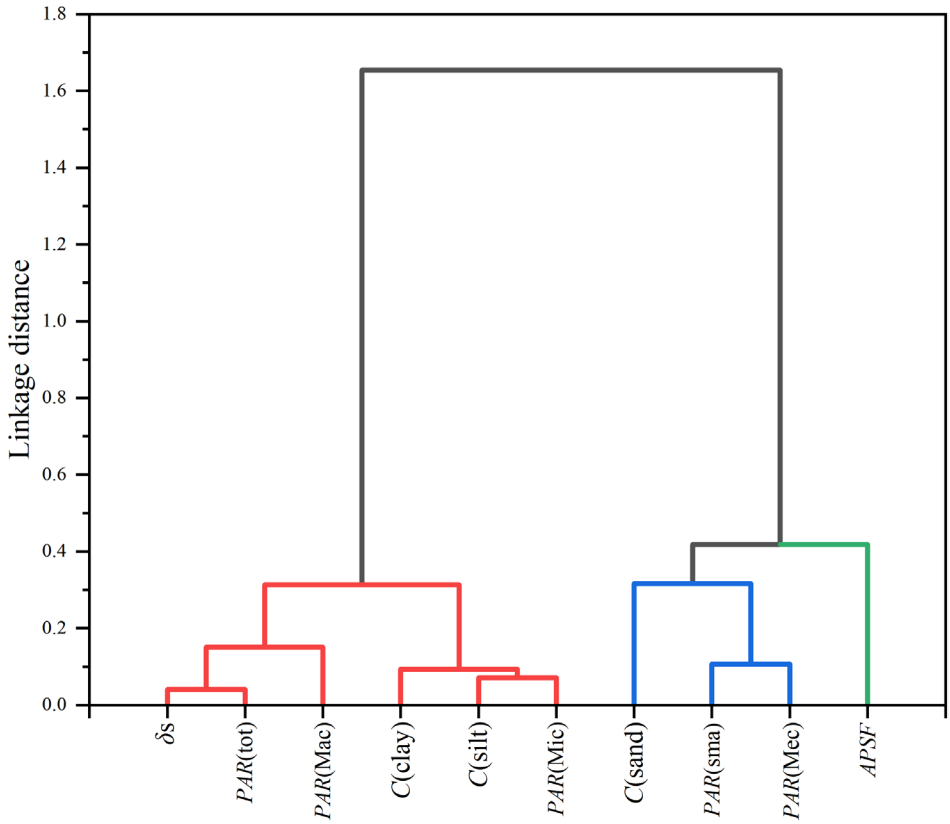

Figure 10. Grouped dendrograms of specimens.

3.6. Microstructural mechanism of freeze–thaw-enhanced collapsibility

The results indicate that the effect of freeze–thaw cycling on the wetting-induced collapse behavior of Xinjiang loess is essentially a process of progressive microstructural destabilization (Yang *et al.* 2025). Repeated freeze–thaw action promoted aggregate disintegration and particle refinement, as reflected by the increase in clay and silt fractions and the reduction in sand content. More importantly, it induced substantial pore-system reconstruction, including an increase in total pore area ratio, a marked rise in macropore content, a reduction in mesopores, and a decrease in pore roundness. These changes indicate that the original metastable loess fabric gradually evolved from a relatively compact mesopore-dominated structure into a more open, irregular, and heterogeneous pore network. Such microstructural degradation directly explains the increase in wetting-induced collapse. Under unsaturated conditions, the original aggregated skeleton can remain stable due to matric suction and interparticle support. However, repeated freeze–thaw cycling progressively weakens this metastable framework by disrupting aggregate integrity, opening the pore system, and increasing structural heterogeneity. Once wetted under vertical load, the weakened skeleton can no longer maintain its original arrangement, leading to rapid particle rearrangement, pore collapse, and structural compression. This is consistent with the observed increase in the collapsibility coefficient at 200 kPa, particularly after 5–7 freeze–thaw cycles, when the most pronounced microstructural deterioration was identified. The statistical analyses further support this mechanism. Pearson correlation analysis showed that the collapsibility coefficient was most strongly associated with total pore area ratio and macropore area ratio, while mesopore area ratio was negatively correlated with collapse response. PCA identified a dominant structural mode controlled mainly by particle refinement, pore-system opening, macropore development, and increasing pore irregularity. HCA yielded a consistent result, clustering the collapsibility coefficient most closely with macropore area ratio and total pore area ratio. Taken together, these results indicate that the enhancement of wetting-induced collapse under freeze–thaw cycling was governed primarily by pore-system opening and structural coarsening, whereas particle-size redistribution and pore-shape modification acted as secondary factors. Therefore, the mechanism of freeze–thaw-enhanced collapsibility in Xinjiang loess can be summarized as follows: repeated freezing and thawing progressively destroy the original metastable aggregated structure, promote particle refinement and pore-network opening, and generate a looser and more unstable skeleton. When wetted under load, this weakened structure undergoes intensified pore collapse and particle rearrangement, ultimately resulting in a significant increase in wetting-induced collapse deformation (Wang and Li 2024).

3.7. Broader geoscientific implications

Although this study focuses on the collapsibility of Xinjiang loess from a geotechnical perspective, the results also provide insight into the response of continental near-surface materials to cyclic climatic forcing (Pye 1995).

In seasonally frozen arid and semi-arid regions, freeze–thaw action can progressively modify the fabric, pore structure, and water sensitivity of shallow loess deposits. The observed transition from a relatively intact aggregated fabric to a more open and macropore-rich structure indicates that repeated freeze–thaw cycling may increase the susceptibility of loess-covered terrains to wetting-induced deformation, slope instability, and surface settlement (Wang and Cheng 2023). More broadly, this study highlights the need to connect climatic processes with microstructural evolution when evaluating the long-term stability of surficial deposits. The combined use of collapse testing, SEM observation, image-based pore quantification, and multivariate analysis provides a useful framework for tracing how environmental forcing is translated into structural weakening and mechanical response (Javier *et al.* 2013). This perspective may also be relevant for other climate-sensitive unconsolidated deposits subjected to repeated freeze–thaw and wetting disturbances.

4. Conclusions

This study investigated the effect of freeze–thaw cycling on the wetting-induced collapse behavior of Xinjiang loess through collapsibility tests, particle-size analysis, SEM observation, quantitative pore-structure characterization, and multivariate statistical analysis. The main conclusions are as follows:

(1) Freeze–thaw cycling enhanced the wetting-induced collapse behavior of Xinjiang loess in a stage-dependent manner. The collapsibility coefficient at 200 kPa increased overall from 0.0809 in the untreated state to 0.115 after 10 cycles. The response was not strictly linear, with limited changes after 1–3 cycles but a pronounced increase during 5–7 cycles, indicating a transition from early local disturbance to more extensive structural weakening.

(2) Repeated freeze–thaw cycling induced progressive microstructural degradation of the loess, manifested by aggregate disintegration, particle refinement, increased total pore area ratio, marked macropore development, reduced mesopore content, and more irregular pore geometry. These changes indicate that the original metastable fabric gradually evolved into a looser, more open, and more heterogeneous structure.

(3) SEM observation, particle-size analysis, and quantitative pore characterization consistently indicated that the 5–7 cycle interval represented a key microstructural transition stage. During this stage, aggregate disintegration, macropore development, mesopore reduction, and pore-shape irregularity became more evident, corresponding closely to the strongest increase in collapsibility.

(4) Pearson correlation analysis, PCA, and HCA consistently showed that the increase in collapsibility was more strongly associated with pore-system opening and structural coarsening than with particle-size redistribution alone. In particular, the total pore area ratio and macropore area ratio showed the closest association with the collapsibility coefficient within the present dataset. These results support a microstructure-based interpretation that freeze–thaw-enhanced collapsibility is mainly linked to nonlinear pore-system reconstruction and macropore development.

Data availability statement

The data that support the findings of this study, including collapsibility test results, particle-size distribution data, SEM images, and Avizo-derived pore-structure data, are available from the corresponding author upon reasonable request.

Declaration of generative AI and AI-assisted technologies

During the preparation of this manuscript, the authors used ChatGPT only to improve language, readability, and the presentation of limited sections of the manuscript. Generative AI was not used for data generation, data analysis, interpretation of results, or the development of scientific conclusions. The authors take full responsibility for the content of the manuscript.

Acknowledgments

This study was substantially supported by the General projects of the Shaanxi Province Natural Science Basic Research Program (2025JC-YBQN-435), China Postdoctoral Science Foundation (Grant No. 2024MD753992), Shaanxi Geotechnical Mechanics and Engineering Young Talent Support Program Project (Grant No. YESS2024005), the National Natural Science Foundation of China (Grant No. 42372320, Grant No. 41972292), the Innovation Capability Support Program of Shaanxi Province (Grant No. 2021TD-54) and the Key Research and Development Projects of Shaanxi Province (Grant No. 2022ZDLSF06-03).

Authors' contribution

Kangze Yuan: conceptualization, methodology, investigation, formal analysis, funding acquisition, writing—original draft; Wanli Xie: conceptualization, methodology, supervision, funding acquisition, writing—review and editing; Jiahao Zhou: investigation; Xuanyu Gao: investigation; Qiqi Liu: investigation; Xinyu Li: investigation. All authors have read and agreed to the published version of the manuscript.

Conflicts of interest

The authors declare that they have no known competing financial interests or personal relationships that could have appeared to influence the work reported in this paper.

References

ASTM. Standard practice for classification of soils for engineering purposes (unified soil classification system). 2006a. Available: https://www.scribd.com/document/488180059/ASTM-D2487-11-Classification-of-Soils-for-Engineering-Purposes-Unified-Soil-Classification-System-pdf (accessed on 8 January 2026).

ASTM. Standard test methods for laboratory compaction characteristics of soil using modified effort. 2006b. Available: https://store.astm.org/d1557-07.html (accessed on 10 January 2026).

Bai J. *The early Precambrian geology of Wutaishan*. Tianjin: Tianjin Science and Technology Press, 1986.

Bai R, Lai Y, Zhang M, Jiang H. Investigating the thermo-hydro-mechanical behavior of loess subjected to freeze–thaw cycles. *Acta Geotech.* 2024, 19(9):6305–6318. DOI: 10.1007/s11440-024-02306-y

Besson M, Metian M, Bustamante P, Hédouin L. Metal(loid)s in superficial sediments from coral reefs of French Polynesia. *Mar. Pollut. Bull.* 2020, 155:111175. DOI: 10.1016/j.marpolbul.2020.111175

Della Vecchia G, Dieudonné A, Jommi C, Charlier R. Accounting for evolving pore size distribution in water retention models for compacted clays. *Int. J. Numer. Anal. Methods Geomech.* 2015, 39(7):702–723. DOI: 10.1002/nag.2326

Gao C, Wu Z, Chen R, Ma Y. Impact of freeze-thaw cycles on loess microstructure: a comparison of fine-grained and coarse-grained

soils. *Cold Reg. Sci. Technol.* 2025a, 241:104701. DOI: 10.1016/j.coldregions.2025.104701

Gao X, Xie W, Yuan K, Liu Q. Mechanical properties and microstructural evolution of Malan loess with depth: insights from multivariate statistical models. *Soil Tillage Res.* 2025b, 251:106548. DOI: 10.1016/j.still.2025.106548

Hou K, Qian H, Zhang Y, Qu W, Ren W, *et al*. Relationship between fractal characteristics of grain-size and physical properties: insights from a typical loess profile of the loess Plateau. *Catena* 2021, 207:105653. DOI: 10.1016/j.catena.2021.105653

Javier L, Woodroffe C, Phinn SR, Hamylton S, Callagan DP, *et al*. A sediment budget for Lizard Island, northern Great Barrier Reef. In *Proceedings of the 8th International Conference on Geomorphology (AIG) "Geomorphology and Sustainability"*, Paris, France, August 27–31, 2013, pp. 840–840.

Kim JK, Kim EH, Lee OK, Park SY, Lee B, *et al*. Variation and correlation analysis of phenolic compounds in mungbean (Vigna radiata L.) varieties. *Food Chem.* 2013, 141(3):2988–2997. DOI: 10.1016/j.foodchem.2013.05.060

Lei X. Pore type of loess in China and collapsibility. *Sci. Sin. B* 1987, 17:1309–1316.

Leng Y, Peng J, Wang Q, Meng Z, Huang W. A fluidized landslide occurred in the Loess Plateau: a study on loess landslide in South Jingyang tableland. *Eng. Geol.* 2018, 236:129–136. DOI: 10.1016/j.enggeo.2017.05.006

Li G, Wang F, Ma W, Fortier R, Mu Y, *et al*. Variations in strength and deformation of compacted loess exposed to wetting-drying and freeze-thaw cycles. *Cold Reg. Sci. Technol.* 2018, 151:159–167. DOI: 10.1016/j.coldregions.2018.03.021

Li J, Wang K, Wang Q, Liu X, Zhao Z. Early Proterozoic collision orogenic belt in Wutaishan area, China (In Chinese). *Chin. J. Geol.* 1990, 25(1):1–11.

Li P, Pan Z, Xiao T, Wang J. Effects of molding water content and compaction degree on the microstructure and permeability of compacted loess. *Acta Geotech.* 2023, 18(2):921–936. DOI: 10.1007/s11440-022-01592-8

Ma H, Gu T, Cui B, Li S, Tang Y, *et al*. Surface subsidence patterns and mechanisms of underlying goaf beneath a railway tunnel. *Cont. Life Evol.* 2026, 1(1):1–17. DOI: 10.55092/cle20260003

Münker C. Nb/Ta fractionation in a Cambrian arc/back arc system, New Zealand: source constraints and application of refined ICP-MS techniques. *Chem. Geol.* 1998, 144(1–2):23–45. DOI: 10.1016/S0009-2541(97)00105-8

Musso G, Azizi A, Jommi C. A microstructure-based elastoplastic model to describe the behaviour of a compacted clayey silt in isotropic and triaxial compression. *Can. Geotech. J.* 2020, 57(7):1025–1043. DOI: 10.1139/cgj-2019-0176

Pearce JA. Basalt geochemistry used to investigate past tectonic environments on Cyprus. *Tectonophysics* 1975, 25(1–2):41–67. DOI: 10.1016/0040-1951(75)90010-4

Pearce JA, Cann JR. Tectonic setting of basic volcanic rocks determined using trace element analyses. *Earth Planet. Sci. Lett.* 1973, 19(2):290–300. DOI: 10.1016/0012-821X(73)90129-5

Pearce JA, Flower MF. The relative importance of petrogenetic variables in magma genesis at accreting plate margins: a preliminary investigation. *J. Geol. Soc.* 1977, 134(2):103–127. DOI: 10.1144/gsjgs.134.2.0103

Porter SC. Loess records | China. *In Encyclopedia of Quaternary Science*. Oxford: Elsevier. 2007. pp. 1429–1440.

Pye K. The nature, origin and accumulation of loess. *Quat. Sci. Rev.* 1995, 14(7–8):653–667. DOI: 10.1016/0277-3791(95)00047-X

Radelyuk I, Tussupova K, Persson M, Zhapargazinova K, Yelubay M. Assessment of groundwater safety surrounding contaminated water storage sites using multivariate statistical analysis and Heckman selection model: a case study of Kazakhstan. *Environ. Geochem. Health* 2021, 43(2):1029–1050. DOI: 10.1007/s10653-020-00685-1

Rubatto D, Hermann J. Zircon formation during fluid circulation in eclogites (Monviso, Western Alps): implications for Zr and Hf budget in subduction zones. *Geochim. Cosmochim. Acta* 2003, 67(12):2173–2187. DOI: 10.1016/S0016-7037(02)01321-2

Shao X, Zhang H, Tan Y. Collapse behavior and microstructural alteration of remolded loess under graded wetting tests. *Eng. Geol.* 2018, 233:11–22. DOI: 10.1016/j.enggeo.2017.11.025

Stolz A, Jochum KP, Spettel B, Hofmann AW. Fluid- and melt-related enrichment in the subarc mantle: evidence from Nb/Ta variations in island-arc basalts. *Geology* 1996, 24(7):587–590. DOI: 10.1130/0091-7613(1996)024<0587:FAMREI>2.3.CO;2

Sun D, Li Q, Liu S, Chen X, Wang Z. Neoarchean-Paleoproterozoic magmatic arc evolution in the Wutai-Hengshan-Fuping area, North China Craton: new perspectives from zircon U–Pb ages and Hf isotopic data. *Precambrian Res.* 2019, 331:105368. DOI: 10.1016/j.precamres.2019.105368

Tian Z, Song K, Yan X, Zhang Z, Zhang Y, *et al*. Exploring rainfall effects on the Xingfu Dayuan Landslide in Yecheng, Xinjiang, China using time-series InSAR technology and numerical simulation. *Sci. Rep.* 2026, 16(1):14876. DOI: 10.1038/s41598-026-45241-6

Tiwari N, Satyam N, Sharma M. Micro-mechanical performance evaluation of expansive soil biotreated with indigenous bacteria using MICP method. *Sci. Rep.* 2021, 11(1):10324. DOI: 10.1038/s41598-021-89687-2

Vecchia GD, Romero E. A fully coupled elastic–plastic hydromechanical model for compacted soils accounting for clay activity. *Int. J. Numer. Anal. Methods Geomech* 2013, 37(5):503–535. DOI: 10.1002/nag.1116

Wang K, Zhou S, Hao J. The metamorphism and significance of kyanite-bearing assemblages from the original Jingangku formation of Wutaishan area. *Acta Petrol. Sin.* 1996, 12(1):88–98.

Wang Q, Wang J, Li S, Li S, Li C, *et al*. Experiments to simulate the salinisation process of loess under a dynamic water cycle. *Environ. Res.* 2025, 268:120739. DOI: 10.1016/j.envres.2024.120739

Wang S, Lv Q, Baaj H, Li X, Zhao Y. Volume change behaviour and microstructure of stabilized loess under cyclic freeze–thaw conditions. *Can. J. Civ. Eng.* 2016, 43(10):865–874. DOI: 10.1139/cjce-2016-0052

Wang Y, Cheng H. Advances in microscopic pore structure characterization of fine-grained mudrocks. *Energy Fuels* 2023, 37(3):1495–1510. DOI: 10.1021/acs.energyfuels.2c03144

Wang Y, Li Y. Wetting-induced collapse of loess: tracing microstructural evolution. *Eng. Geol.* 2024, 340:107673. DOI: 10.1016/j.enggeo.2024.107673

Wilde SA, Zhao G, Wang K, Sun M. First SHRIMP zircon U-Pb ages for Hutuo Group in Wutaishan: further evidence for Palaeoproterozoic amalgamation of North China Craton. *Chin. Sci. Bull.* 2004, 49:83–90. DOI: 10.1007/BF02901747

Wood DA. The application of a Th-Hf-Ta diagram to problems of tectonomagmatic classification and to establishing the nature

of crustal contamination of basaltic lavas. *Earth Planet. Sci. Lett.* 1980, 50(1):11–30. DOI: 10.1016/0012-821X(80)90116-8

Xu J, Li Y, Lan W, Wang S. Shear strength and damage mechanism of saline intact loess after freeze-thaw cycling. *Cold Reg. Sci. Technol.* 2019, 164:102779. DOI: 10.1016/j.coldregions.2019.05.005

Xu P, Zhang Q, Qian H, Qu W, Li M. Microstructure and permeability evolution of remolded loess with different dry densities under saturated seepage. *Eng. Geol.* 2021, 282:105875. DOI: 10.1016/j.enggeo.2020.105875

Yang H, Xie W, Liu Q, Zhu R, Liu Y. Three-stage collapsibility evolution of Malan loess in the Loess Plateau. *Catena* 2022, 217:106482. DOI: 10.1016/j.catena.2022.106482

Yang Y, Gao J, Zhao Y, Qin Y. Field experimental study on the melt sinking characteristics of saline soil in the Qaidam Basin. *Eng. Geol.* 2025, 108431. DOI: 10.1016/j.enggeo.2025.108431

Yuan K, Xie W, Gao X, Li X, Liu Q. From waste to strength: the role of FGD gypsum in loess stabilization and its environmental benefits. *iScience* 2025a, 28(11):113909. DOI: 10.1016/j.isci.2025.113909

Yuan K, Ni W, Della Vecchia G, Lü X, Wang H, *et al*. Influence of dry density and wetting–drying cycles on the soil–water retention curve of compacted loess: experimental data and modeling. *Acta Geotech.* 2024, 19(12):8111–8128. DOI: 10.1007/s11440-024-02354-4

Yuan K, Wang H, Ni W, Ren S, Guo Y. New insights into the dynamic changes of loess collapsibility under climate-induced wetting–drying cycles: a case study of the loess Plateau of China. *Catena* 2025b, 250:108782. DOI: 10.1016/j.catena.2025.108782

Yuan W, Fan W. Quantitative study on the microstructure of loess soils at micrometer scale via X-ray computed tomography. *Powder Technol.* 2022, 408:117712. DOI: 10.1016/j.powtec.2022.117712

Zhao J, Zhou M. Geochemistry of Neoproterozoic mafic intrusions in the Panzhihua district (Sichuan Province, SW China): implications for subduction-related metasomatism in the upper mantle. *Precambrian Res.* 2007, 152(1–2):27–47. DOI: 10.1016/j.precamres.2006.09.002

Zhao L, Peng J, Ma P, Leng Y, Ma Z. Microstructure response to shear strength deterioration in loess after freeze-thaw cycles. *Eng. Geol.* 2023, 323:107229. DOI: 10.1016/j.enggeo.2023.107229

Zheng H, Chen H, Cao J. Palaeoenvironmental implication of the Plio-Pleistocene loess deposits in southern Tarim Basin. *Chin. Sci. Bull.* 2002, 47(8):700–704. DOI: 10.1007/BF02902833

Zhou Z, Ma W, Zhang S, Mu Y, Li G. Effect of freeze-thaw cycles in mechanical behaviors of frozen loess. *Cold Reg. Sci. Technol.* 2018, 146:9–18. DOI: 10.1016/j.coldregions.2017.11.011